Applied Physics Letters ARTICLE scitation.org/journal/apl

Charge collection in *h*-BN neutron detectors at elevated temperatures

Cite as: Appl. Phys. Lett. **118**, 092102 (2021); doi: 10.1063/5.0044159
Submitted: 14 January 2021 · Accepted: 18 February 2021 ·
Published Online: 5 March 2021

View Online Export Citation CrossMark

J. Li, A. Maity, S. J. Grenadier, J. Y. Lin, and H. X. Jiang[a)]

AFFILIATIONS

Department of Electrical and Computer Engineering, Texas Tech University, Lubbock, Texas 79409, USA

[a)]Author to whom correspondence should be addressed: hx.jiang@ttu.edu

ABSTRACT

Many of the neutron detector applications are in the environments with harsh conditions such as high temperatures. We report here the measurements of charge collection parameters of hexagonal boron nitride (*h*-BN) detectors at elevated temperatures, including the electron mobility-lifetime product ($\mu\tau$) and surface recombination field (s/μ). It was found that $\mu\tau$ is increased, while s/μ is decreased as temperature increases. The temperature dependence of the surface recombination field (s/μ) revealed that electrons trapped in the surface states tend to thermally activate to the bulk region at higher temperatures with an activation energy of about 0.22 eV, leading to a reduction in the density of the charged surface states at elevated temperatures. Consequently, the charge collection efficiency is enhanced at elevated temperatures due to a reduced surface recombination field and increased electron mobility-lifetime product. The results suggested that *h*-BN neutron detectors are favorable for high temperature operation.

Hexagonal boron nitride (*h*-BN) has been under intensive investigation in recent years due to its unique properties, such as wide bandgap,[1–7] high emission efficiency,[8–16] high chemical and temperature stability,[17] as well as large thermal neutron capture cross section of the isotope boron-10 (B-10).[18,19] It is a very promising material for deep ultraviolet (DUV) photonic devices[1–16,20–22] and neutron detection applications.[22–29] Neutron detectors with a detector area as large as 1 cm^2 have been fabricated from B-10 enriched *h*-BN (*h*-^{10}BN) epilayers and have demonstrated a record high detection efficiency among solid-state detectors at 59%.[24–27] The attainment of 1 cm^2 detectors with a nearly 60% detection efficiency[27] is a critical step toward the ultimate commercial adoption of *h*-BN neutron detector technology because such solid-state detectors are capable of providing an overall detection sensitivity of 0.6 CPS/NV (neutron counts per second per cm^2), which is equivalent to that of a commercial detector product based on ^{3}He gas tube with a diameter of 1.6 cm pressurized at 2 atm (e.g., Ludlum Model 2241-4 Neutron Dose Survey Meter). However, He-3 gas detectors are most appropriate for operation below 175 °C. With their exceptional characteristics, *h*-^{10}BN neutron detectors are expected to be implemented in many practical application areas, including security, medical, well logging, and life (water) exploration in space. The environments for many of these applications can be extreme and may require devices to operate in severe conditions. For example, in well logging, the temperatures can easily exceed 200 °C. For geothermal logging, the environmental conditions are even more extreme where temperatures can be as high as 500 °C.

The combined mobility-lifetime product has been extensively utilized as an effective tool for correlating the quality and device performance of *h*-^{10}BN neutron detector materials[24–29] as well as for other radiation detector and solar cell materials.[30,31] The mobility-lifetime product can be obtained by measuring and analyzing the photocurrent-applied voltage characteristics using the classical Many's equation under strongly absorbed light illumination.[31] Additionally, the "surface recombination field" or the ratio of surface recombination velocity to mobility ($E_s = s/\mu$) is another key transport parameter that strongly influences the charge collection efficiency and, hence, the overall detection efficiency of *h*-^{10}BN neutron detectors.[24–29] However, these basic transport parameters for *h*-BN have not been investigated at elevated temperatures. We report here the measurements of mobility-lifetime product ($\mu\tau$), surface recombination field (E_s), and their effects on the charge collection efficiency at elevated temperatures up to 425 K for *h*-^{10}BN.

An epilayer of *h*-^{10}BN of ~100 μm in thickness was deposited on a *c*-plane sapphire substrate of 4 in. in diameter, using metal-organic chemical vapor deposition (MOCVD). Based on insights of previous works,[23–25] a low temperature BN buffer layer of ~20 nm in thickness was deposited on a sapphire substrate at 800 °C prior to the growth of the *h*-^{10}BN epilayer, whereas the growth temperature of the subsequent thick h-^{10}BN epilayer was ~1400 °C. The primary purpose of using a reduced growth temperature of 1400 °C and a buffer layer in the present work as compared to the growth temperature of >1400 °C employed in previous works[23–26] was to reduce the effect of oxygen diffusion from the sapphire substrate,[27,28] whereas oxygen impurities in h-BN are known to occupy nitrogen sites (O_N) acting as donors.[27,28] Moreover, layer structured h-BN has a different thermal expansion coefficient than sapphire, enabling natural separation of thick h-BN layers from sapphire substrates during cooling down after epi-growth as well as the attainment of freestanding h-BN epilayers.

A photoconductive-type detector in a lateral geometry was fabricated by affixing a diced piece of h-^{10}BN sample to sapphire using a highly resistive adhesive material. E-beam evaporation was used to deposit the metal bi-layer of Ni (100 nm) and Au (40 nm) on the clipped edges of the h-^{10}BN strip using a shadow mask with metal covering on the edges. Wire bonding was then performed to create an electrical connection between the deposited metal contacts and the pads of a semiconductor device package. A schematic diagram of the cross-sectional view of the h-^{10}BN detector structure used in this work is shown in Fig. 1(a). A microscope image of the fabricated device (with an exposed h-^{10}BN area of 1.8 mm × 4.4 mm) is shown in Fig. 1(b). The dark areas on both sides of the structure are the Ni/Au bilayer metal contacts. A broad-spectrum light source covering the wavelength range between 170 and 2100 nm [model E-99 laser-driven light source (LDLS) by Energytiq] was used as an excitation light source to provide the above bandgap photoexcitation for photocurrent–voltage (I–V) characteristic measurements. Photocurrent was recorded using an electrometer. The temperature of the sample is controlled through a hot plate with a thermal-coupled temperature probe.

To measure the $\mu\tau$ and E_s ($=s/\mu$) as functions of temperature, we focus on the electron transport via the bias scenario and photoexcitation setup shown in Fig. 1(a), in which holes are collected by the negatively biased electrode immediately upon photoexcitation and only electrons are moving inside the epilayer to be collected by the positively biased electrode in a later time. Figure 2 plots the measured I–V curves under the above bandgap photoexcitation at different temperatures. The dotted curves are the measured data and solid curves are the least squares fitting of data with Many's equation:[32]

$$I(V) = I_0\eta_c(V) = I_0\left[\frac{V\mu\tau\left(1-e^{-\frac{L^2}{\mu\tau V}}\right)}{L^2\left(1+\frac{sL}{\mu V}\right)}\right]. \quad (1)$$

Here, the saturation current is denoted as I_0, and $\mu\tau$ and s/μ denote the mobility-lifetime product and the surface recombination field (or the ratio of surface recombination velocity to mobility, $E_s = s/\mu$) for electrons, respectively, whereas $\eta_c(V)$ represents the charge collection efficiency at a bias voltage of V and L is the width of the detector strip. The fitted curves agree very well with measured results and the parameters of electron mobility-lifetime ($\mu\tau$) products and surface recombination field (s/μ or E_s) can thus be obtained at different temperatures.

Figure 3 plots the measured electron mobility-lifetime product ($\mu\tau$) as a function of temperature, which exhibits an increase with temperature from a value of 1.9×10^{-3} cm^2/V at 300 K and reaches a maximum value of 3.6×10^{-3} cm^2/V at T = 375 K. It then decreases with a further increase in temperature. In the temperature range measured between 300 and 425 K, $\mu\tau$ products are all above the room temperature value. Figure 4 plots the measured surface recombination field s/μ as a function of temperature. The solid diamonds are measured data, which reveal a continue decrease in s/μ with temperature increasing. Based on Eq. (1), both behaviors of an increase in $\mu\tau$ product and a decrease in s/μ with temperature imply that the charge collection efficiency is in fact increases with an increase in temperature, which is advantageous for many potential applications.

A decrease in the surface recombination field (s/μ) at higher temperatures can be understood and is related to a decrease in the density of the charged surface states, ρ_{2D}, at higher temperatures. Figure 5 shows a schematic illustration revealing the occurrence of the charged

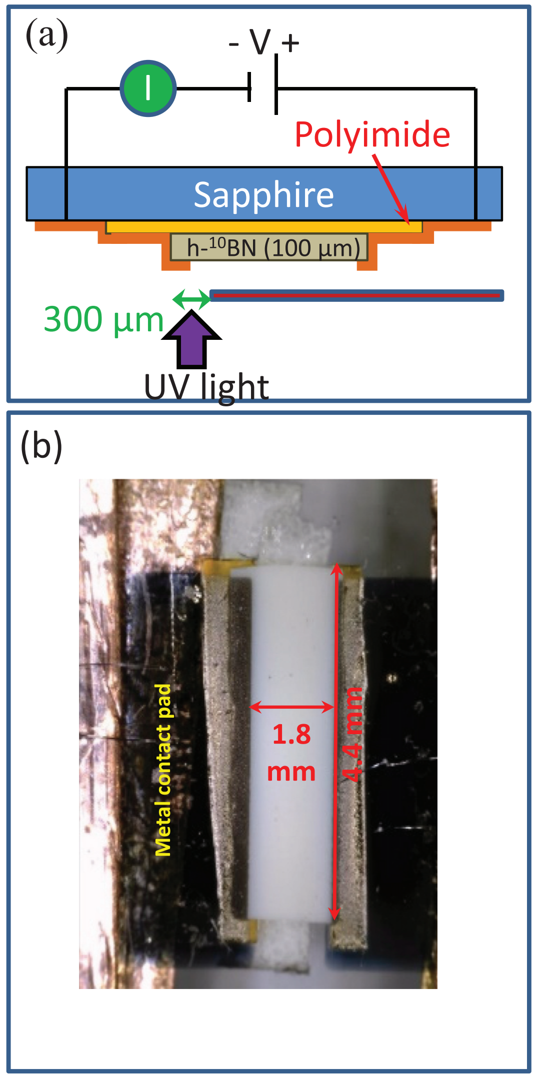

FIG. 1. (a) Schematic illustration of cross-sectional view of a photoconductive type h-^{10}BN detector strip in a lateral geometry and the bias and photoexcitation scenario with UV light illuminated through a metal mask, allowing the measurement of electron transport. (b) Optical microscope image of the h-^{10}BN detector strip with Ni/Au metal bilayer contacts deposited on two edges. The width of the strip is 1.8 mm and the length of the strip is 4.4 mm.

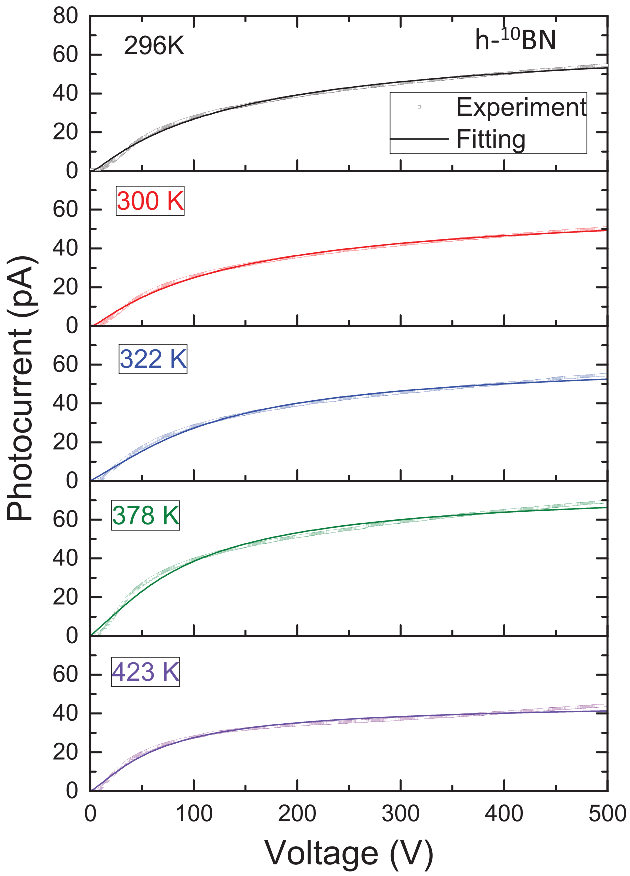

FIG. 2. Photocurrent-voltage characteristics for electrons using the device and bias configuration shown in Fig. 1(a). The solid curves are the least squares fitting using Eq. (1), from which the parameters of electron mobility-lifetime ($\mu\tau$) products and surface recombination field (s/μ or E_s) can be obtained at different temperatures.

surface states due to the presence of ionized impurities or dangling bonds. Negatively charged impurities are present at the surface, while the positively charged donor states are accumulated beneath the surface, forming a depletion region beneath the surface with a width of *d*. Inside this depletion region, there exists an electric field or a potential barrier. Consequently, neutron- or photo-generated free electrons in the bulk region need to overcome this electric field or potential barrier in order to be collected by the electrodes.

The formation of the charged surface states is due to electrons occupying impurity or dangling bond sites at the surface. Assume the total number of surface impurities is N_{2D} at temperature T and the number of surface electrons that will be thermally activated into the depletion region is proportional to $C\exp(-T_0/T)$. Here, C is a constant and is related to the density of states in the bulk. The quantity kT_0 (k is the Boltzmann constant) represents the thermal energy that is sufficient to activate charges from the surface into the bulk. The number of charged surface states at temperature T can thus be expressed as $N_{2D} - C\exp(-T_0/T)$. Since the surface field is directly proportional to the density of charged surface states, we can thus express the surface recombination field E_S (or s/μ) as

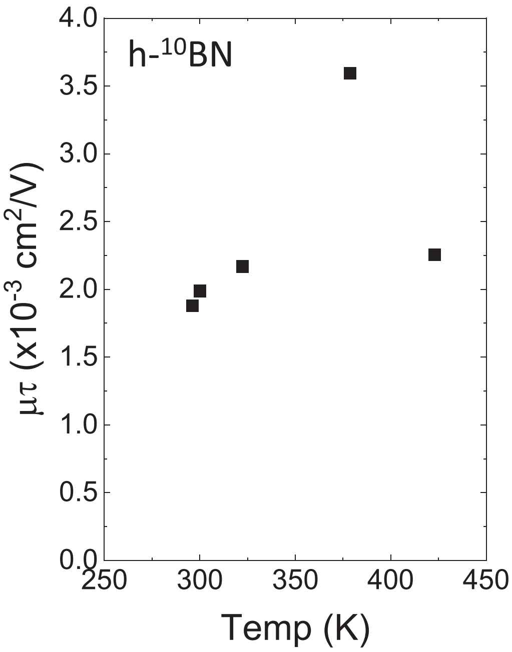

FIG. 3. Measured mobility-lifetime product ($\mu\tau$) as a function of temperature. The $\mu\tau$ product values were obtained from the least squares fitting of the photocurrent-voltage characteristics for electrons with Eq. (1), as shown in Fig. 2.

$$s/\mu = A[1 - B\exp(-T_0/T)], \tag{2}$$

where A and B are two constants, which are fitting parameters. The term of $B\exp(-T_0/T)$ represents the percentage of surface electrons being thermally activated into the bulk region at temperature T, while $[1 - B\exp(-T_0/T)]$ represents the fraction of electrons still occupying the impurity or dangling bond sites at the surface or the percentage of electrons forming the surface states at temperature T. As temperature

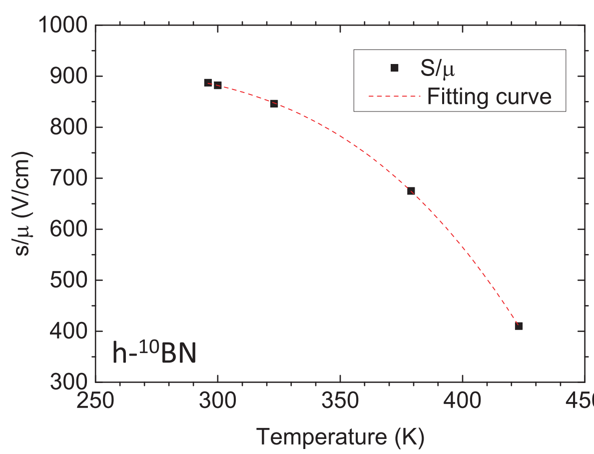

FIG. 4. Measured surface recombination field (s/μ) as a function of temperature and the solid curve is the least squares fitting with Eq. (2). The s/μ values were obtained from the least squares fitting of the photocurrent-voltage characteristics for electrons with Eq. (1), as shown in Fig. 2.

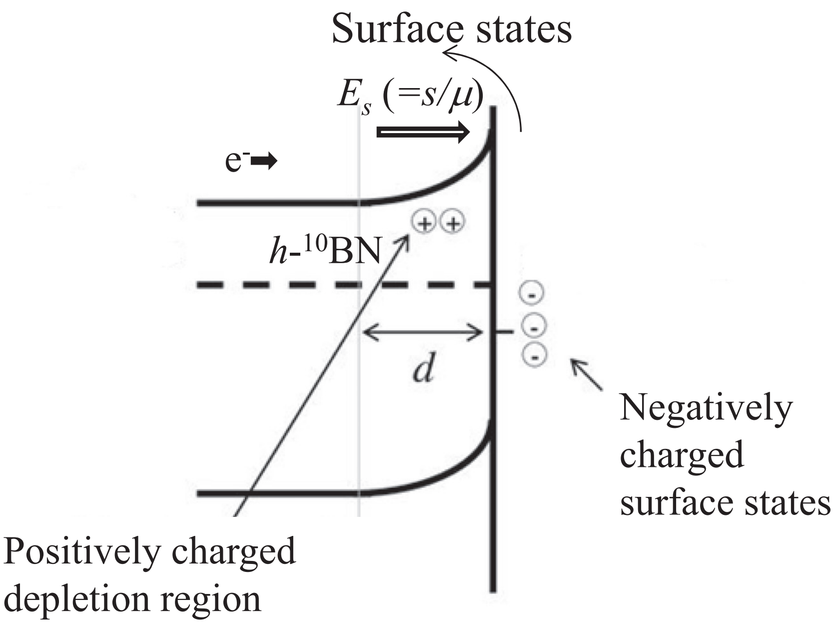

FIG. 5. Illustration of negatively charged surface states and positively charged depletion region near the h-^{10}BN surface. Neutron- or photo-excited electrons must overcome a potential barrier (or electric field) in order to be collected by the metal electrodes.

T approaches to zero, the number of electrons occupying the impurity or dangling bond sites at the surface or the number of charged surface states reaches a maximum.

The dotted curve in Fig. 4 is the least squares fitting of the measured values of s/μ at different temperatures with Eq. (2), which fits well with experimental data. The fitted values of A, B, and T_0 are 920.7 V/cm, 294, and 2654 K ($kT_0 = 0.22$ eV), respectively. In a semiconductor, the presence of the charged surface states is known to "pin" the Fermi level in the bandgap. The results shown in Fig. 4 thus suggest that the density of the charged surface states follows a thermal activation behavior with an activation energy of about 0.22 eV, which equivalently corresponds to an energy barrier that determines the fraction of electrons thermally activated from the surface to the bulk.

Figure 5 is schematic illustration showing the charged surface states and the resulting potential barrier (or electric field) in the depletion region. The surface recombination field (s/μ or E_s) was introduced in the denominator of Eq. (1). From the results obtained above and Fig. 5, the physical meaning of this surface recombination field ($E_s = s/\mu$) becomes more clearer—it is the electric field caused by the charged surface states and the induced depletion region adjacent to it. All neutron and photogenerated electrons in the bulk need to overcome this electric field or potential barrier in order to be collected by the electrodes. The size of this surface recombination field is proportional to the density of the charged surface states. With a decrease in the density of the charged surface states and an increase in $\mu\tau$ products at higher temperatures, the charge collection efficiency increases with an increase in temperature. This is very encouraging in terms of using h-^{10}BN detectors for high temperature applications.

To further understand the behavior of the temperature dependence of the surface recombination field, s/μ or E_s, we noted that this surface field is caused by the presence of negatively charged surface states (electrons occupying at the impurity or dangling bond sites) and the accumulation of positively charged ionized impurities beneath the surface, forming a depletion region with a width d, as illustrated in Fig. 5. There is a potential barrier in this depletion region with an electric field (E_s) changes lineally from 0 to a maximum value of E_{max} at the surface,

$$\mathbf{E_{max}} = (\rho_{2D}/\varepsilon_0\varepsilon_{\parallel})\mathbf{k}_{\parallel}, \tag{3}$$

where $\rho_{2D} = N_{3D}{\cdot}d$ is the density of the charged surface states, $\varepsilon_0 = 8.85 \text{ x } 10^{-12}$ (C/V·m) is the vacuum permittivity, N_{3D} symbolizes the positively charged impurity density in the depletion region, $\varepsilon_{\parallel} = 6.85$ is the in-plane dielectric constant of h-BN, and $\mathbf{k}_{\parallel}$ denotes a unit vector perpendicular to the surface of charge collection. In our case, $\mathbf{k}_{\parallel}$ is parallel to the c-plane and perpendicular to the c-axis of h-^{10}BN crystal.

To estimate the parameters in the depletion region and at the surface, assuming the measured activation energy $E_a = 0.22$ eV is on the same order as the band bending in the depletion region, we thus have $\int_0^d eEdz = (1/2)eE_{max}d = E_a$. Also assume that the measured s/μ at $T \to 0$ represents the average electric field in the depletion region, i.e., s/μ $(T \to 0) = (1/2)E_{max}$, we thus have $E_{max} = 2s/\mu$ $(T = 0) = 2$ A $= 2 \times 920.7$ V/cm $= 1.84 \times 10^3$ V/cm. From the above discussion, the depletion width can be estimated as $d = 2E_a/eE_{max} = 2 \times 0.22$ eV/(e $\times 1.84 \times 10^3$ V/cm) $= 2.4 \times 10^{-4}$ cm $= 2.4\ \mu$m. Moreover, from Eq. (3), we can also deduce the density of the charged surface states, $\rho_{2D} = N_{2D}{\cdot}d = \varepsilon_0\varepsilon_{\parallel}E_{max} = 6.85 \times 8.85 \times 10^{-12}$ (C/V·m) $\times$ (1.84 $\times$ 10^3 V/cm) $= 1.1 \times 10^{-9}$ C/cm^2 $= 6.9 \times 10^9$ e/cm^2. The presence of the charged surface states is the source of the surface recombination field, which strongly influences the charge collection efficiency. Reducing the density of the surface impurities or dangling bonds through surface passivation or avoiding oxidization of the surfaces should reduce the density of the charged surface states as well as the surface recombination field and increase the charge collection efficiency.

In summary, we have investigated key transport parameters and gained a better understanding of the charge collection in h-^{10}BN detectors at elevated temperatures. It was found that the electron mobility-lifetime ($\mu\tau$) product increases and the surface recombination field (s/μ) decreases at elevated temperatures. Consequently, the charge collection efficiency is enhanced at higher temperatures in comparison with that at room temperature. The temperature variation of the surface recombination field (s/μ) can be described very well by a thermal activation behavior of the surface electrons into the bulk. This activation energy and the corresponding depletion width and density of the charged surface states have been deduced. The results are encouraging for potential applications of *h*-BN neutron detectors at high temperatures.

This work was supported by DOE ARPA-E (Grant Nos. DE-AR0000964 and DE-AR0001257). Jiang and Lin are grateful to the AT&T Foundation for the support of Ed Whitacre and Linda Whitacre endowed chairs.

DATA AVAILABILITY

The data that support the findings of this study are available from the corresponding author upon reasonable request.

REFERENCES

[1]A. Zunger, A. Katzir, and A. Halperin, "Optical properties of hexagonal boron nitride," Phys. Rev. B **13**, 5560 (1976).

[2]T. Sugino, K. Tanioka, S. Kawasaki, and J. Shirafuji, "Characterization and field emission of sulfur-doped boron nitride synthesized by plasma-assisted chemical vapor deposition," Jpn. J. Appl. Phys., Part 2 **36**, L463 (1997).

[3]K. Watanabe, T. Taniguchi, and H. Kanda, "Direct-bandgap properties and evidence for ultraviolet lasing of hexagonal boron nitride single crystal," Nat. Mater. **3**, 404 (2004).

[4]Y. Kubota, K. Watanabe, O. Tsuda, and T. Taniguchi, "Deep ultraviolet light-emitting hexagonal boron nitride synthesized at atmospheric pressure," Science **317**, 932 (2007).

[5]K. Watanabe, T. Taniguchi, T. Niiyama, K. Miya, and M. Taniguchi, "Far-ultraviolet plane-emission handheld device based on hexagonal boron nitride," Nat. Photonics **3**, 591 (2009).

[6]X. Z. Du, C. D. Frye, J. H. Edgar, J. Y. Lin, and H. X. Jiang, "Temperature dependence of the energy bandgap of two-dimensional hexagonal boron nitride probed by excitonic photoluminescence," J. Appl. Phys. **115**, 053503 (2014).

[7]X. Z. Du, J. Li, J. Y. Lin, and H. X. Jiang, "Temperature dependence of the energy bandgap of multi-layer hexagonal boron nitride," Appl. Phys. Lett. **111**, 132106 (2017).

[8]K. Watanabe and T. Taniguchi, "Jahn-Teller effect on exciton states in hexagonal boron nitride single crystal," Phys. Rev. B **79**, 193104 (2009).

[9]B. Arnaud, S. Lebègue, P. Rabiller, and M. Alouani, "Huge excitonic effects in layered hexagonal boron nitride," Phys. Rev. Lett. **96**, 026402 (2006); "Arnaud, Lebègue, Rabiller, and Alouani Reply," **100**, 189702 (2008).

[10]L. Museur and A. Kanaev, "Near band-gap photoluminescence properties of hexagonal boron nitride," J. Appl. Phys. **103**, 103520 (2008).

[11]L. Wirtz, A. Marini, and A. Rubio, "Excitons in boron nitride nanotubes: Dimensionality effects," Phys. Rev. Lett. **96**, 126104 (2006).

[12]L. Wirtz, A. Marini, M. Gruning, C. Attaccalite, G. Kresse, and A. Rubio, "Comment on 'Huge excitonic effects in layered hexagonal boron nitride'," Phys. Rev. Lett. **100**, 189701 (2008).

[13]X. K. Cao, B. Clubine, J. H. Edgar, J. Y. Lin, and H. X. Jiang, "Two-dimensional excitons in three-dimensional hexagonal boron nitride," Appl. Phys. Lett. **103**, 191106 (2013).

[14]B. Huang, X. K. Cao, H. X. Jiang, J. Y. Lin, and S. H. Wei, "Origin of the significantly enhanced optical transitions in layered boron nitride," Phys. Rev. B **86**, 155202 (2012).

[15]S. Majety, X. K. Cao, J. Li, R. Dahal, J. Y. Lin, and H. X. Jiang, "Band-edge transitions in hexagonal boron nitride epilayers," Appl. Phys. Lett. **101**, 051110 (2012).

[16]J. Li, S. Majety, R. Dahal, W. P. Zhao, J. Y. Lin, and H. X. Jiang, "Dielectric strength, optical absorption, and deep ultraviolet detectors of hexagonal boron nitride epilayers," Appl. Phys. Lett. **101**, 171112 (2012).

[17]Z. Liu, Y. Gong, W. Zhou, L. Ma, J. Yu, J. C. Idrobo, J. Jung, A. H. MacDonald, R. Vajtai, J. Lou, and P. M. Ajayan, "Ultrathin high-temperature oxidation-resistant coatings of hexagonal boron nitride," Nat. Commun. **4**, 2541 (2013).

[18]G. F. Knoll, *Radiation Detection and Measurement*, 4th ed. (John Wiley & Sons, 2010).

[19]O. Osberghaus, "Die isotopenhäufigkeit des bors. Massenspektrometrische untersuchung der elektronenstoßprodukte von BF_3 und BCl_3," Z. Phys. **128**, 366 (1950).

[20]R. Dahal, J. Li, S. Majety, B. N. Pantha, X. K. Cao, J. Y. Lin, and H. X. Jiang, "Epitaxially grown semiconducting hexagonal boron nitride as a deep ultraviolet photonic material," Appl. Phys. Lett. **98**, 211110 (2011).

[21]H. X. Jiang and J. Y. Lin, "Hexagonal boron nitride for deep ultraviolet photonic devices (in special section 'Deep UV LEDs,' Guest editors: Jung Han, Hiroshi Amano and Leo Scholwalter)," Semicon. Sci. Technol. **29**, 084003 (2014).

[22]T. C. Doan, J. Li, J. Y. Lin, and H. X. Jiang, "Growth and device processing of hexagonal boron nitride epilayers for thermal neutron and deep ultraviolet detectors," AIP Adv. **6**, 075213 (2016).

[23]J. Li, R. Dahal, S. Majety, J. Y. Lin, and H. X. Jiang, "Hexagonal boron nitride epitaxial layers as neutron detector materials," Nucl. Inst. Methods Phys. Res. A **654**, 417 (2011).

[24]A. Maity, S. J. Grenadier, J. Li, J. Y. Lin, and H. X. Jiang, "Hexagonal boron nitride neutron detectors with high detection efficiencies," J. Appl. Phys. **123**, 044501 (2018).

[25]A. Maity, S. J. Grenadier, J. Li, J. Y. Lin, and H. X. Jiang, "Effects of surface recombination on the charge collection in h-BN neutron detectors," J. Appl. Phys. **125**, 104501 (2019).

[26]A. Maity, S. J. Grenadier, J. Li, J. Y. Lin, and H. X. Jiang, "High sensitivity hexagonal boron nitride lateral neutron detectors," Appl. Phys. Lett. **114**, 222102 (2019).

[27]A. Maity, S. J. Grenadier, J. Li, J. Y. Lin, and H. X. Jiang, "High efficiency hexagonal boron nitride neutron detectors with 1 cm^2 detection areas," Appl. Phys. Lett. **116**, 142102 (2020).

[28]S. J. Grenadier, A. Maity, J. Li, J. Y. Lin, and H. X. Jiang, "Origin and roles of oxygen impurities in hexagonal boron nitride epilayers," Appl. Phys. Lett. **112**, 162103 (2018).

[29]S. J. Grenadier, A. Maity, J. Li, J. Y. Lin, and H. X. Jiang, "Lateral charge carrier transport properties of B-10 enriched hexagonal BN thick epilayers," Appl. Phys. Lett. **115**, 072108 (2019).

[30]T. Takahashi and S. Watanabe, "Recent progress in CdTe and CdZnTe detectors," IEEE Trans. Nucl. Sci. **48**, 950 (2001).

[31]N. Beck, N. Wyrsch, C. Hof, and A. Shah, "Mobility lifetime product—A tool for correlating a-Si:H film properties and solar cell performances," J. Appl. Phys. **79**, 9361 (1996).

[32]A. Many, "High-field effects in photoconducting cadmium sulphide," J. Phys. Chem. Solids **26**, 575 (1965).